Journal of
Synchrotron Radiation

ISSN 0909-0495

Received 2 May 2007
Accepted 11 June 2007

Probing atomic displacements with thermal differential EXAFS

M. P. Ruffoni,[a]* R. F. Pettifer,[a] S. Pascarelli,[a] A. Trapananti[a] and O. Mathon[a]

[a]Department of Physics, University of Warwick, Coventry CV4 7AL, UK, and [b]European Synchrotron Radiation Facility, 6 Rue Jules Horowitz, BP 220, 38043 Grenoble CEDEX, France. E-mail: ruffoni@esrf.fr

Differential extended X-ray absorption fine structure (DiffEXAFS) is a novel technique for the study of small atomic strains. Here the development of this technique to the measurement of thermally induced strain is presented. Thermal DiffEXAFS measurements have been performed on α-Fe and SrF_2, yielding $\alpha = (11.6 \pm 0.4) \times 10^{-6}\,K^{-1}$ and $(19 \pm 2) \times 10^{-6}\,K^{-1}$, respectively. These are in good agreement with accepted values, proving the viability of the technique. Analysis has revealed sensitivity to mean atomic displacements of 0.3 fm.

Keywords: differential EXAFS; atomic displacements; thermal modulation.

1. Introduction

Differential extended X-ray absorption fine structure (DiffEXAFS) is a novel technique for the study of small atomic strains that has recently been developed by Pettifer *et al.* (2005). Taking a sample where the fundamental structure is known, the technique employs a dispersive-geometry X-ray spectrometer to measure subtle changes in absorption fine structure induced by the modulation of a given sample property. This allows changes in photoelectron scattering path length to be found, and thus any atomic perturbations in the local area of the absorbing atom (Ruffoni *et al.*, 2007).

In this work we present the results of thermal expansion measurements conducted using thermal DiffEXAFS, where samples undergo temperature modulation of the order of 1 K. For the first such measurements of this nature, we chose to study iron and strontium fluoride under ambient conditions given that their thermal characteristics are well understood, and thus would serve to assess the viability and accuracy of the technique. Previous DiffEXAFS measurements (focusing exclusively on magnetostrictive phenomena) have directly resolved mean atomic displacements of the order of 1 fm (Pettifer *et al.*, 2005), 100 times more sensitive than is typically possible with standard EXAFS techniques (Dalba *et al.*, 1999). Here we report sensitivity to mean atomic displacements of 0.3 fm.

2. Theory

Since DiffEXAFS is concerned with small changes in the sample material, the anticipated signal may be found from a first-order Taylor expansion of the EXAFS fine-structure function with respect to the modulated sample property. For thermal studies the signal has two components, one from net expansion of the sample, and another from changes to the disorder of each atom.

The spherically averaged thermally dependent EXAFS fine-structure function

$$\chi(k, T) = \sum_j A_j(k) \exp\left[-2k^2\sigma_j^2(T)\right] \sin\left[s_j(T)k + \varphi_j(k)\right] \quad (1)$$

thus yields

$$\Delta\chi = \sum_j A_j \exp\left(-2k^2\sigma_j^2\right)\left[k\cos\left(ks_j + \varphi_j\right)\Delta s_j - 2k^2 \sin\left(ks_j + \varphi_j\right)\Delta\sigma_j^2\right], \quad (2)$$

where j covers all scattering paths of length s_j, including multiple scattering, $A_j(k)$ is an amplitude function, $\sigma_j^2(T)$ is the Debye–Waller factor for structural disorder, and $s_j(T)k + \varphi_j(k)$ is the scattering phase. Strictly speaking, $A_j(k)$ and $\varphi_j(k)$ are also thermally dependent, but their variations are negligible compared with $\sigma_j^2(T)$ and $s_j(T)$, respectively. Δs_j describes thermally induced net changes in scattering path length. In the absence of any non-linear phenomena such as phase transitions, this just arises from thermal expansion in the sample. $\Delta\sigma_j^2$ represents changes to the Debye–Waller factor and thus thermal disorder.

Both equations (1) and (2) model thermal expansion, and thus asymmetry of the atomic pair-potential, within the quasi-harmonic approximation of Leibfried & Ludwig (1961). In this sense, given that ΔT is small for DiffEXAFS, the harmonic Gaussian pair-potential typically used in EXAFS is retained, but its centroid displaced to model anharmonicity arising from thermal expansion.

Given that the fundamental structure of the sample is known beforehand, fitting (2) to experimental data deals with a strictly limited number of parameters; positions of atoms are fixed, and thus shell radii and coordination numbers. Consequently, $A_j(k)$ and $\varphi_j(k)$ may be determined from first princi-

ples, and σ_j^2 from a conventional EXAFS fit, leaving only the perturbations Δs_j and $\Delta\sigma_j^2$ to be determined from the DiffEXAFS.

Examining (2), it is clear that the disorder term retains the sine phase dependency of the original fine-structure function (1), whereas the expansion term has changed to a cosine dependency. Contributions from thermal disorder are therefore in phase with the conventional EXAFS, whilst those from thermal expansion are in quadrature. This difference is key in allowing each term to be resolved in an experimental DiffEXAFS spectrum.

It can also be seen that both terms scale with photoelectron wavevector: expansion by k and disorder by k^2. This indicates that both terms are amplified relative to the conventional EXAFS as X-ray energy increases, resulting in more high-k oscillations being present in the DiffEXAFS compared with the conventional fine structure, in turn allowing DiffEXAFS data to be acquired further from the edge.

Inserting the thermal expansion coefficient for each path α_j, and considering the possibility of non-unit-temperature modulation, (2) becomes

$$\Delta\chi/\Delta T = \sum_j A_j(k)\exp\left(-2k^2\sigma_j^2\right)\left\{ks_j\cos\left[ks_j+\varphi_j(k)\right]\alpha_j/\Delta T - 2k^2\sin\left[ks_j+\varphi_j(k)\right]\Delta\sigma_j^2/\Delta T\right\}. \quad (3)$$

Each coefficient is assumed to be temperature independent since ΔT is only of the order of one 1 K.

The α_j may be analysed in the context of the geometry of path j in order to obtain the second-rank thermal expansion tensor α_{mn}. Each tensor coefficient is determined by the analysis of a scattering path with geometry sensitive to strains along the same direction described by the coefficient. Some paths, particularly multiple-scattering paths, may be sensitive to strains described by two or more coefficients.

However, the point-group crystal symmetry of a chosen sample material can be exploited through von Neumann's principle to reduce the number of independent coefficients (Nye, 1985). For crystals of cubic symmetry as used here, the tensor is isotropic. Thus α_j is the same for every scattering path.

Note also that in inserting α_j into (2) an additional factor, s_j, is introduced. This reveals the last key property of the differential fine-structure function: thermal expansion in larger scattering paths is amplified relative to shorter ones. High-order paths therefore hold comparatively greater significance than they would do in conventional EXAFS. Critically, the thermal-disorder term does not scale with s_j, so when s_j is large the thermal expansion component of the differential fine structure becomes a greater fraction of the total observed signal.

Given that typical values of $\Delta\sigma_j^2$ are roughly an order of magnitude greater than α_j, thermal DiffEXAFS signals will be largely in phase with the conventional EXAFS, thermal expansion being manifest as a small phase-shift.

3. Experimental

DiffEXAFS experiments were performed on ID24, the Dispersive-EXAFS beamline of the ESRF (Pascarelli *et al.*, 2006). Mounted on a third-generation undulator source and producing a wavelength-dispersive beam corresponding to an energy range of several hundred eV, ID24 allows an entire EXAFS spectrum to be acquired simultaneously. Averaging pairs of 200 ms acquisition measurements over a few hours according to Mathon *et al.* (2004) yields fractional errors in $\Delta\chi$ of about 10^{-5}. Temperature modulation was performed by passing one of two jets of heated N_2 gas over samples with a small thermal mass, contained within a thermally isolated environment as shown schematically in Fig. 1.

Gas from a dry nitrogen source was passed into a fast-switching two-way fluidic valve mounted at the rear of the apparatus. Simply by passing a high or low voltage signal to the valve, gas was switched to flow down separate channels and into one of two identical aluminium heat sinks.

The temperature of each heat sink was set by a Peltier effect heater (PEH) mounted on top of it. Also mounted on the heat sink was a silicon band-gap temperature sensor, which, along with PEH, were connected to a proportional integral derivative (PID) controller that then actively regulated the power in the PEH so as to maintain a constant temperature in the heat sink. The desired temperature was selected on the PID controller to a precision of 0.1 K and then maintained electronically to an accuracy of ± 0.2 K.

With this arrangement, temperature modulation was achieved by setting the two heat-sink PID controllers to slightly different temperatures and then switching the two-way valve back and forth so as to cycle the gas flow through each heat sink alternately. Since the temperature of the heat sinks themselves did not require modulation between each XAS measurement, the thermal stability of the gas jets was high. Given also that the two heat sinks were totally independent, the output gas jet temperature could be cycled in a reproducible fashion upon switching of the valve.

The temperature of the sample material itself was recorded for each spectrum acquisition using a small copper-constantan thermocouple attached to it. The time required for the sample

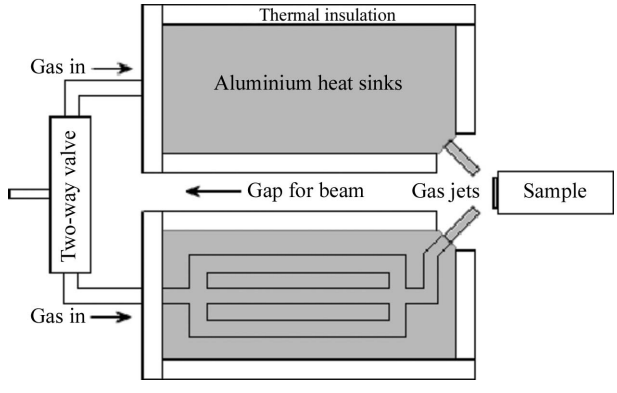

Figure 1
A schematic representation of the gas jet apparatus used for this thermal DiffEXAFS experiment.

to reach equilibrium with a changed gas temperature was approximately 1–2 s depending on the sample and the degree of temperature change.

4. Results and discussion

Fig. 2 shows a plot of both the Fe *K*- and Sr *K*-edge EXAFS (scaled in amplitude) and the associated thermal DiffEXAFS for modulation of the order of 1 K at room temperature. The time between measurements at $T+$ and $T-$ was 1.5 s for the Fe measurements and 3 s for the Sr measurements, with each pair of measurements repeated 600 times and averaged to minimize statistical noise. Each complete difference measurement was repeated with the initial gas jet phase reversed, causing all observed structure to invert about $\Delta\chi = 0$, proving its thermal origin. These spectra have themselves been inverted and plotted as the grey lines on Fig. 2. Additional control measurements with $\Delta T = 0.0$ K yielded no structure larger than that anticipated from our 0.2 K error in setting the gas jet temperatures, further demonstrating that the signals are thermally generated.

A strong dominance of the DiffEXAFS disorder component is clearly observed given the signals are largely in phase with the EXAFS. However, the vertical dashed-grey lines, which are centred on the three largest EXAFS peaks, reveal that the DiffEXAFS spectra are phase shifted, indicating that the thermal expansion component has also been detected. As ΔT increases, so does the amplitude of the difference signal. Normalizing each to a 1 K unit-temperature modulation yields the differential EXAFS, which shows that the amplitude follows a linear scaling relationship with temperature as predicted by (3).

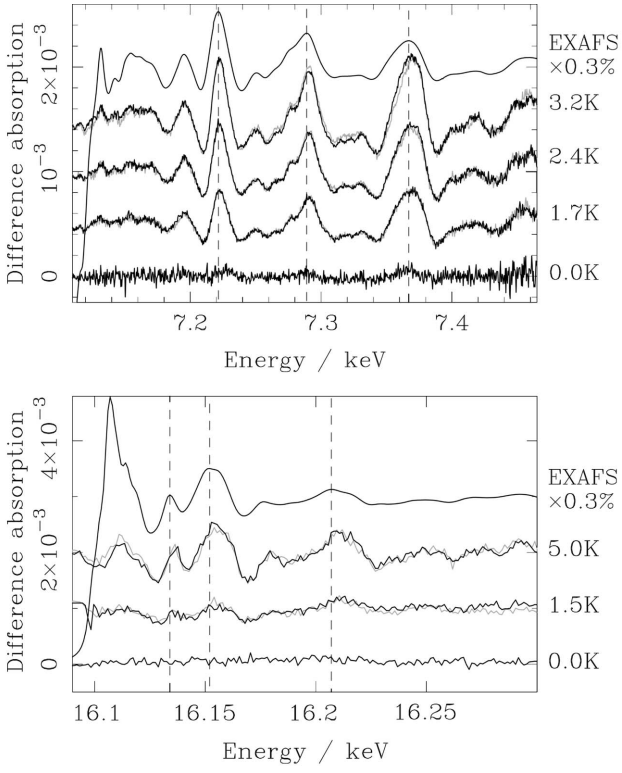

Figure 2
Experimental EXAFS and DiffEXAFS for the Fe and Sr *K*-edges of α-Fe (top graph) and SrF_2 (bottom graph) at room temperature. ΔT for each difference spectrum is shown on the right, and is set to an accuracy of ± 0.2 K. The grey plots are the inverted gas jet phase-reversed signals, which are essentially identical to the black plots, proving the thermal origin of the signal. The dashed vertical lines, which are centred on peaks in the EXAFS plots, highlight the phase shift of the difference signals with respect to the EXAFS.

The absence of any sharp features at the edge energy, where the XAFS derivative is maximal, is testament to energy stability between $T+$ and $T-$ measurements of better than 10 meV as required (Pettifer *et al.*, 2005). Also noticeable, especially in the Fe data, is the k and k^2 dependency of the DiffEXAFS expansion and disorder terms, respectively. Whereas the three marked peaks in the EXAFS plot become progressively smaller with increasing energy, the same peaks in the DiffEXAFS plots are all of similar amplitude. Additionally, the s_j dependency of the thermal expansion term is visible by virtue of the additional high-frequency structure, seen between the primary peaks of the DiffEXAFS data, but which are absent from the conventional EXAFS.

For analysis of the Fe data, the fine-structure phase, $s_j(T)k + \varphi_j(k)$, and amplitude, $A_j(k)$, components in (1) were calculated from *ab initio* theory in the range $0 \leq k \leq 20$ Å^{-1} using the *FEFF* code (version 8.28) (Rehr & Albers, 2000). The α-Fe body-centred cubic (b.c.c.) crystal structure supplied to *FEFF* was generated using the lattice parameter at room temperature, $a = 2.8665$ Å (Pearson, 1958). Atomic potentials were modelled according to Hedin & Lundqvist (1969). Calculated scattering paths (which included multiple-scattering paths) were filtered, limiting the minimum path amplitude to 4% of the largest path amplitude and the maximum half path length, R, to 5.0 Å. This left 12 significant paths out to and including the fifth coordination shell.

Using this information, the absolute σ_j^2 for each of these paths were then obtained from a fit to a normal Fe *K*-edge EXAFS spectrum, acquired on BM29, the conventional step-scanning XAS beamline of the ESRF. For the first three single scattering paths, these were $\sigma_1 = (6.5 \pm 0.2) \times 10^{-3}$ Å^2, $\sigma_2 = (5.8 \pm 0.2) \times 10^{-3}$ Å^2 and $\sigma_3 = (7.2 \pm 0.4) \times 10^{-3}$ Å^2, respectively. This spectrum was Fourier filtered to limit R to 5.0 Å, matching the path length filter used in *FEFF*. The structure was again fixed to a b.c.c. structure with $a = 2.8665$ Å. This fit also served to establish the fine-structure amplitude reduction factor, S_0^2, and a correction to the calculated edge energy, ΔE_0. Once this fit was complete, all absolute structural parameters in (3) were known. Fixing these parameters then provided a reference point from which to measure the perturbations observed in the DiffEXAFS.

The experimental DiffEXAFS spectra were Fourier filtered, again to the region $0.0 \leq R \leq 5.0$ Å. Theory DiffEXAFS spectra, generated from the paths calculated by *FEFF*, and with the information obtained from the conventional EXAFS fit, were then fitted to these experimental spectra in order to determine α and $\Delta\sigma_j^2/\Delta T$. The subscript j is dropped on α through von Neumann's Principle, and the same coefficient fitted to each path. Although 12 paths were considered, only

the first four single-scattering paths were found to contribute significantly to the DiffEXAFS signal.

The noise in the data was estimated by assuming that it was white, and was purely statistical for Fourier components corresponding to $R \geq 30$ Å. No low-R filter was imposed to remove the absorption background. Instead, background features were subtracted using a six-coefficient Chebyshev polynomial incorporated into the fit.

Rather than filtering the noise in R-space, the Fourier transform relation $R = \pi/2\Delta k$ was used to fit smoothed piecewise-continuous natural cubic splines, with knots positioned such that Δk corresponded to $R = 30$ Å, to the spectra to define the EXAFS components. The fit residuals then defined the noise. This approach is more favourable to Fourier filtering since it allows us to preserve the k-dependence of the noise.

The analysis process for the SrF_2 data was very similar. Given the SrF_2 lattice parameter $a = 5.7996$ Å (Swanson *et al.*, 1955), *FEFF* generated the scattering phase and amplitude information. Filtering limited paths to no more than 7.5 Å in length, and required their amplitude to be at least 1.5% of the amplitude of the largest path.

$\sigma_j^2(T)$, S_0^2 and ΔE_0 were obtained from a fit to the conventional Sr K-edge structure [giving $\sigma_1 = (9.6 \pm 0.1) \times 10^{-3}$ Å^2, $\sigma_2 = (7 \pm 3) \times 10^{-3}$ Å^2 and $\sigma_3 = (10.4 \pm 0.4) \times 10^{-3}$ Å^2, respectively, for the first three single-scattering paths]. The DiffEXAFS were Fourier filtered to $0 \leq R \leq 4.57$ Å, leaving three significant paths: the first three single-scattering paths. Theory was again fitted to the experimental DiffEXAFS to obtain α and $\Delta\sigma_j^2/\Delta T$. The noise was extracted based on a maximum EXAFS scattering radius of 15 Å.

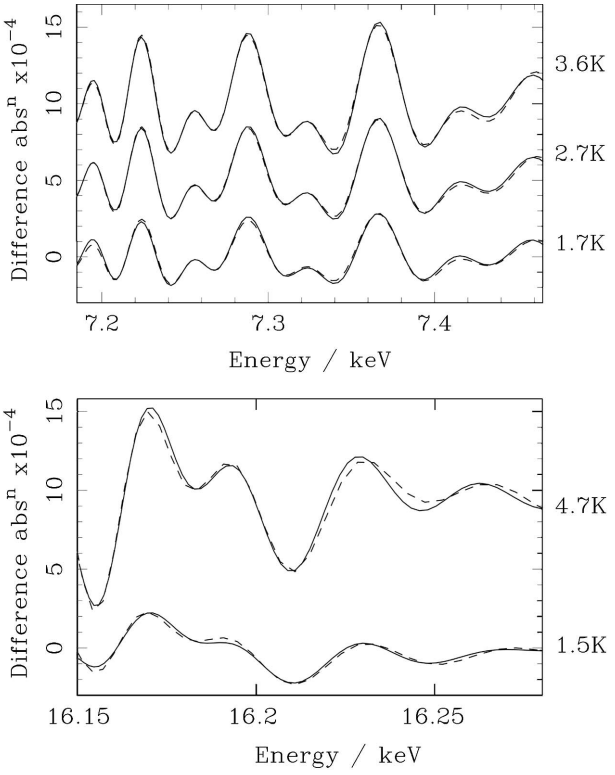

Figure 3
Fourier-filtered experimental DiffEXAFS spectra (solid line) for α-Fe (top graph) and SrF_2 (bottom graph), which have been fitted to the DiffEXAFS fine-structure function (3) (dashed line). ΔT for each spectrum is given on the right. The associated fit parameters are shown in Table 1.

Table 1
DiffEXAFS parameters for α-Fe and SrF_2.

α is in units of 10^{-6} K^{-1} and $\Delta\sigma_j^2/\Delta T$ in 10^{-5} Å^2 K^{-1}. Note that errors for α and $\Delta\sigma_j^2$ are based on the fit errors only and do not include possible errors from ΔT.

Fe DiffEXAFS	ΔT (K)		
	1.7 ± 0.2	2.7 ± 0.2	3.6 ± 0.2
α	11.1 ± 0.9	12.1 ± 0.6	11.5 ± 0.5
$\Delta\sigma_1^2/\Delta T$	1.48 ± 0.04	1.38 ± 0.03	1.33 ± 0.02
$\Delta\sigma_2^2/\Delta T$	1.34 ± 0.08	1.04 ± 0.06	1.09 ± 0.04
$\Delta\sigma_3^2/\Delta T$	2.2 ± 0.1	1.60 ± 0.07	1.47 ± 0.06
$\Delta\sigma_4^2/\Delta T$	2.0 ± 0.1	1.5 ± 0.1	1.38 ± 0.08

SrF_2 DiffEXAFS	ΔT (K)	
	1.5 ± 0.2	4.7 ± 0.2
α	20 ± 3	18 ± 1
$\Delta\sigma_1^2/\Delta T$	2.04 ± 0.09	1.85 ± 0.05
$\Delta\sigma_2^2/\Delta T$	3.1 ± 0.4	2.0 ± 0.2
$\Delta\sigma_3^2/\Delta T$	2.2 ± 0.5	3.4 ± 0.2

Fig. 3 shows the theory fit to experiment for the filtered Fe and SrF_2 DiffEXAFS data based on (3). The corresponding parameters are shown in Table 1. The non-monotonic trend in $\Delta\sigma_j^2/\Delta T$ with increasing j in Fe, although not in agreement with harmonic models of atomic vibrations, are consistent with recent Born–von Karman lattice dynamics calculations performed by Jeong *et al.* (2003).

Averaging the thermal expansion coefficient for each sample material over all its DiffEXAFS measurements yields $\alpha = (11.6 \pm 0.4) \times 10^{-6}$ K^{-1} for Fe and $\alpha = (19 \pm 2) \times 10^{-6}$ K^{-1} for SrF_2, which agree with the accepted values of $\alpha = 11.8 \times 10^{-6}$ K^{-1} and $\alpha = 18.1 \times 10^{-6}$ K^{-1}, respectively (Nix & MacNair, 1941; Roberts & White, 1986). Given the error of 5×10^{-7} K^{-1} in the Fe thermal expansion coefficient over an average ΔT of 2.6 K, we claim to be able to resolve thermally induced atomic displacements to an accuracy of about 0.3 fm.

5. Conclusions

DiffEXAFS is a viable technique for the measurement of thermally induced strains. Here we have demonstrated the measurement of thermal expansion in some simple materials, and have shown that the microscopic expansion coefficient is the same as its macroscopic counterpart. However, the technique presented may be applied to more complex crystalline systems or even amorphous systems with minimal changes. The potential for studying amorphous systems presents numerous opportunities where other techniques struggle. The true power of thermal DiffEXAFS, however, will lie in the measurement of non-linear phenomena such as phase transitions. With displacements detectable over temperature

changes of about 1 K, high-resolution measurements of atomic motion may be made through transition regions, which until now has not been possible by any other X-ray spectroscopic technique.

The authors would like to thank D. Sutherland, and A. Sheffield for the manufacture of our gas jet apparatus, A. Lovejoy for the design and manufacture of the accompanying electronics, and S. Pasternak and F. Perrin for technical support at the ESRF.

References

Dalba, G., Fornasini, P., Grisenti, R. & Purans, J. (1999). *Phys. Rev. Lett.* **82**, 4240–4243.
Hedin, L. & Lundqvist, S. (1969). *Solid State Physics*, edited by F. Seitz, D. Turnbull & H. Ehrenreich, Vol. 23, pp. 1–181. New York: Academic Press.
Jeong, I.-K., Heffner, R. H., Graf, M. J. & Billinge S. J. L. (2003). *Phys. Rev. B*, **67**, 104301.
Leibfried, G. & Ludwig, W. (1961). *Solid State Phys.* **12**, 275.
Mathon, O., Baudelet, F., Itié, J.-P., Pasternak, S., Polian, A. & Pascarelli, S. (2004). *J. Synchrotron Rad.* **11**, 423–427.
Nix, F. C. & MacNair, D. (1941). *Phys. Rev.* **60**, 597–605.
Nye, J. F. (1985). *Physical Properties of Crystals: Their Representation by Tensors and Matricies*, pp. 20–24. Oxford University Press.
Pascarelli, S., Mathon, O., Muñoz, M., Mairs, T. & Susini, J. (2006). *J. Synchrotron Rad.* **13**, 351–358.
Pearson, W. B. (1958). *A Handbook of Lattice Spacings and Structures of Metals and Alloys.* New York: Pergamon Press.
Pettifer, R. F., Mathon, O., Pascarelli, S., Cooke, M. D. & Gibbs, M. R. J. (2005). *Nature (London)*, **435**, 78–81.
Rehr, J. J. & Albers, R. C. (2000). *Rev. Mod. Phys.* **72**, 621–654.
Roberts, R. B. & White, G. K. (1986). *J. Phys. C*, **19**, 7167–7172.
Ruffoni, M. P., Pettifer, R. F., Pascarelli, S., Trapananti, A. & Mathon, O. (2007). *13th International Conference on X-ray Absorption Fine Structure*, edited by B. Hedman, pp. 838–841. Melville, NY: American Institute of Physics.
Swanson, H. E., Gilfrich, N. T. & Ugrinic, G. M. (1955). *Standard X-ray Diffraction Powder Patterns*, No. 539, Vol. 5. Washington, DC: National Bureau of Standards.